https://dx.doi.org/10.1021/acs.nanolett.0c01011

Overcoming Nanoparticle-Mediated Complement Activation by Surface PEG Pairing

Martina Pannuzzo, Sara Esposito, Lin-Ping Wu, Jaehong Key, Santosh Aryal, Christian Celia, Luisa di Marzio, Seyed Moein Moghimi,* and Paolo Decuzzi*

ABSTRACT: Many PEGylated nanoparticles activate the complement system, which is an integral component of innate immunity. This is of concern as uncontrolled complement activation is potentially detrimental and contributes to disease pathogenesis. Here, it is demonstrated that, in contrast to carboxyPEG$_{2000}$-stabilized poly(lactic-*co*-glycolic acid) nanoparticles, surface camouflaging with appropriate combinations and proportions of carboxyPEG$_{2000}$ and methoxyPEG$_{550}$ can largely suppress nanoparticle-mediated complement activation through the lectin pathway. This is attributed to the ability of the short, rigid methoxyPEG$_{550}$ chains to laterally compress carboxyPEG$_{2000}$ molecules to become more stretched and assume an extended, random coil configuration. As supported by coarse-grained molecular dynamics simulations, these conformational attributes minimize statistical protein binding/intercalation, thereby affecting sequential dynamic processes in complement convertase assembly. Furthermore, PEG pairing has no additional effect on nanoparticle longevity in the blood and macrophage uptake. PEG pairing significantly overcomes nanoparticle-mediated complement activation without the need for surface functionalization with complement inhibitors.

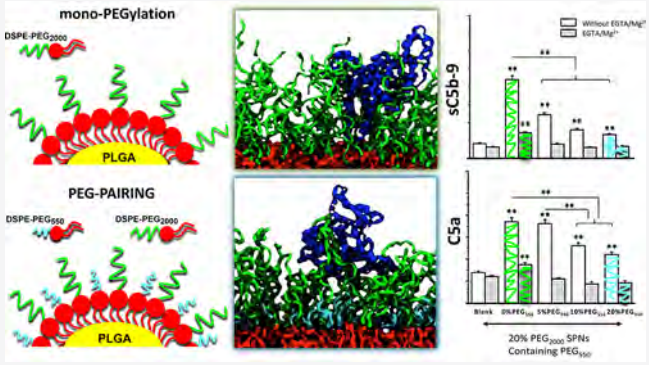

KEYWORDS: *nanoparticles, surface engineering, PEG conformation, protein absorption, complement lectin pathway*

The complement system is an enzymatic defense cascade.[1] Complement activation can prime particulate intruders with opsonic C3b and iC3b components, which aid their recognition by the blood leukocytes and tissue macrophages.[1,2] Surface camouflaging of nanoparticles with hydrophilic polymers, such as poly(ethylene glycol) (PEG) and related copolymers, reduces complement activation, but polymer surface density and conformation apparently regulate the mode of complement activation.[3−7] For instance, changes in surface polymer architecture from "mushroom" to intermediary "mushroom-brush" and "brush-like" configurations not only reduce the extent of complement activation but also further shift complement activation from the classical and alternative pathways to the lectin pathway.[3] Changes in polymer conformation may affect the extent, the type, and the mode of protein binding, where some bound proteins through conformational changes trigger complement activation or expose functionalities that allow protein−C3 adduct formation (opsonization).[6,7] Thus, such dynamic processes might explain the differential complement activation phenomenon.[6] However, the total bound proteins do not determine the efficacy of complement activation and C3 opsonization.[7]

Improved surface engineering initiatives are therefore needed to suppress nonspecific blood protein deposition. which in turn may diminish or overcome complement activation. When a protein molecule approaches the surface of a polymer-coated nanoparticle, the number of available conformations of surface-projected polymer chains is reduced due to compression or interpenetration of polymer chains.[8] This develops an osmotic repulsive force due to loss of conformational freedom of the polymer chains. If the polymer surface density is high, it is probable that compression is preferred to interpenetration, whereas if the density is low, interpenetration is likely to dominate. Therefore, surface conditions that generate polymer compression may reduce complement activation processes due to lesser protein intercalation.[8,9] Here, we have tested this hypothesis through a "polymer-pairing" surface engineering process (combinations of short and long PEG chains), as such

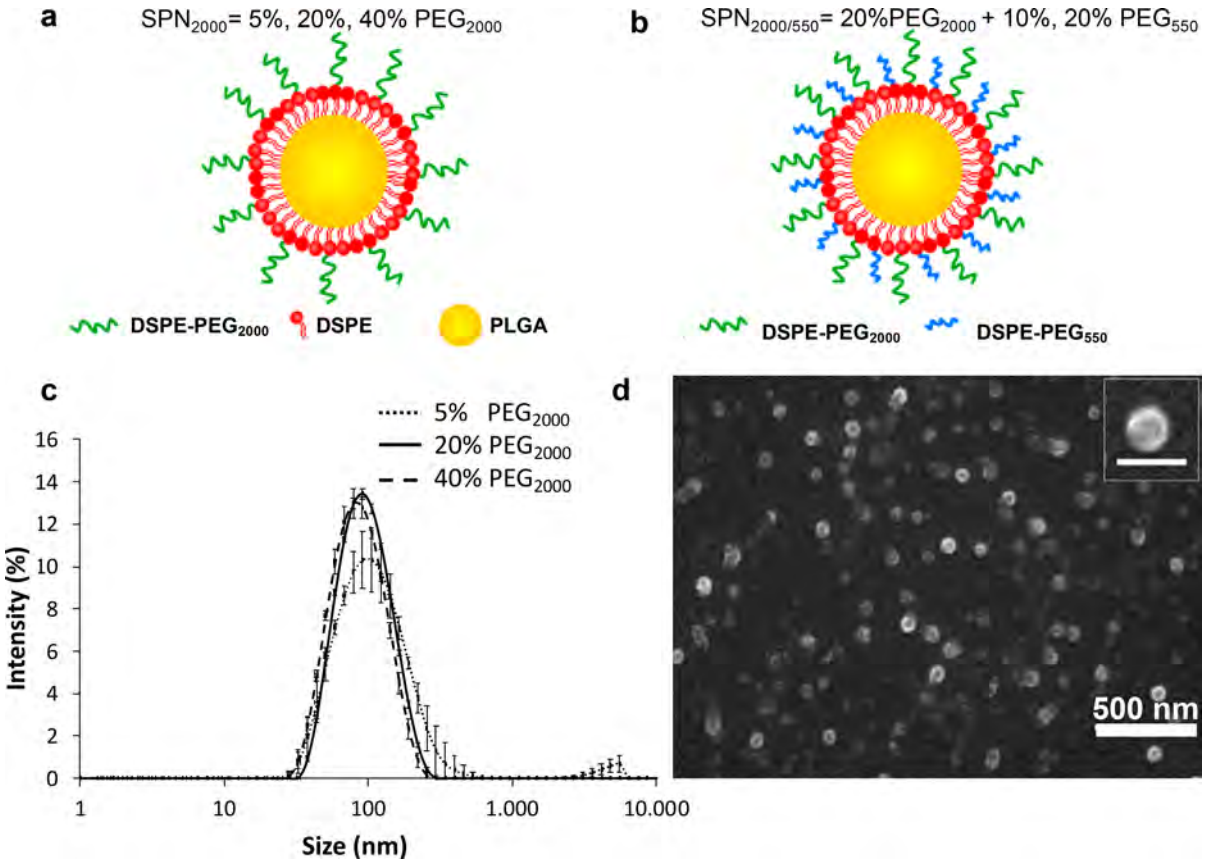

Figure 1. Geometrical configuration and physicochemical characterization of SNP_{2000} and $SNP_{2000/550}$. Schematic representation of conventional SNP_{2000} consisting of a poly(lactic acid-*co*-glycolic acid) (PLGA) core, a lipid monolayer shell, and a hydrophilic coating of carboxyPEG_{2000}-phospholipid chains on the surface (PEG_{2000}-DSPE). (b) Schematic representation of PEG-paired $SNP_{2000/550}$ consisting of a PLGA core, a lipid monolayer shell, and a hydrophilic coating of carboxyPEG_{2000}-phospholipid and methoxyPEG_{550}-phospholipid chains on the surface (PEG_{2000}-DSPE and PEG_{550}-DSPE). (c) Hydrodynamic diameter (nm) of SNPs with different carboxyPEG_{2000} contents, measured by dynamic light scattering. (d) Representative scanning electron micrograph of SNP_{2000}. The scale bar in the inset is 100 nm.

combinations can modulate projected polymer chain conformation and distancing.[10]

Spherical PEGylated poly(lactic-*co*-glycolic acid) (PLGA) nanoparticles (SPNs) were considered as a reference system. These nanoparticles have been extensively tested in vitro and in vivo for diverse biomedical and targeting applications.[11−13] SPNs were synthesized via an established nanoprecipitation method,[11] resulting in a hydrophobic core of PLGA externally stabilized by a monolayer of 1,2-distearoyl-*sn*-glycero-3-phosphoethanolamine (DSPE) and 1,2-distearoyl-*sn*-glycero-3-phosphoethanolamine-carboxy-PEG_{2000} conjugate (carboxy-PEG_{2000}-DSPE). The carboxylic acid functionality was chosen as earlier studies suggested that nanoparticle-mediated complement activation in human sera may be minimized depending on the carboxylic acid surface density and patterning, which could promote factor H binding (a complement control protein, which processes cofactor activity for factor-I-mediated C3b cleavage).[14,15] In line with these suggestions, our preliminary experiments with PEGylated liposomes has further confirmed the superiority of carboxy-terminated PEGs over their methoxy-terminated counterparts in suppressing complement activation (Figure S1). Furthermore, carboxylic functionality may allow for PEG conformational sensing/shielding through electrophoretic mobility measurements. Two different SPN preparations were synthesized: SPN_{2000}, which are surface-decorated nanoparticles with carboxy-PEG_{2000}-DSPE (PEG M_w = 2000 Da); $SPN_{2000/550}$, which are surface-decorated nanoparticles with a combination of carboxyPEG_{2000}-DSPE and methoxyPEG_{550}-DSPE (PEG M_w = 550 Da). The methoxy functionality was chosen for PEG_{550}-DSPE to minimize electrostatic interactions with smaller proteins that might penetrate through the carboxyPEG_{2000} cloud. In the SPN_{2000} preparation, the carboxyPEG_{2000}-DSPE concentration varied between 5 and 40% of the total nanoparticle weight. In the case of $SPN_{2000/550}$, a library of nanoparticles was generated by pairing a fixed amount of carboxyPEG_{2000}-DSPE (20% of the total particle weight) with varying quantities of methoxyPEG_{550}-DSPE, ranging from 5 to 20% of the total nanoparticle weight. A schematic representation for the two SPN preparations is provided in Figure 1a,b. In the sequel, PEG_{2000}, herein, is considered with a carboxy termination, whereas PEG_{550} is referred to have a methoxy termination.

The SPN size distribution was examined by both dynamic light scattering (DLS) and nanoparticle tracking analysis (NTA). Typical DLS size distribution profiles are provided in Figure 1c and in Figure S2, whereas particle sphericity is confirmed by electron microscopy (Figure 1d). No significant change in SPN mean hydrodynamic size was detected by DLS with increasing PEG_{2000} and PEG_{550} levels. For SPN_{2000}, the hydrodynamic diameter ranged between 64.0 ± 9.0 and 70.0 ± 10.0 nm, whereas for $SPN_{2000/550}$, the hydrodynamic diameter varied between 56.0 ± 1.0 and 60.0 ± 2.0 nm.

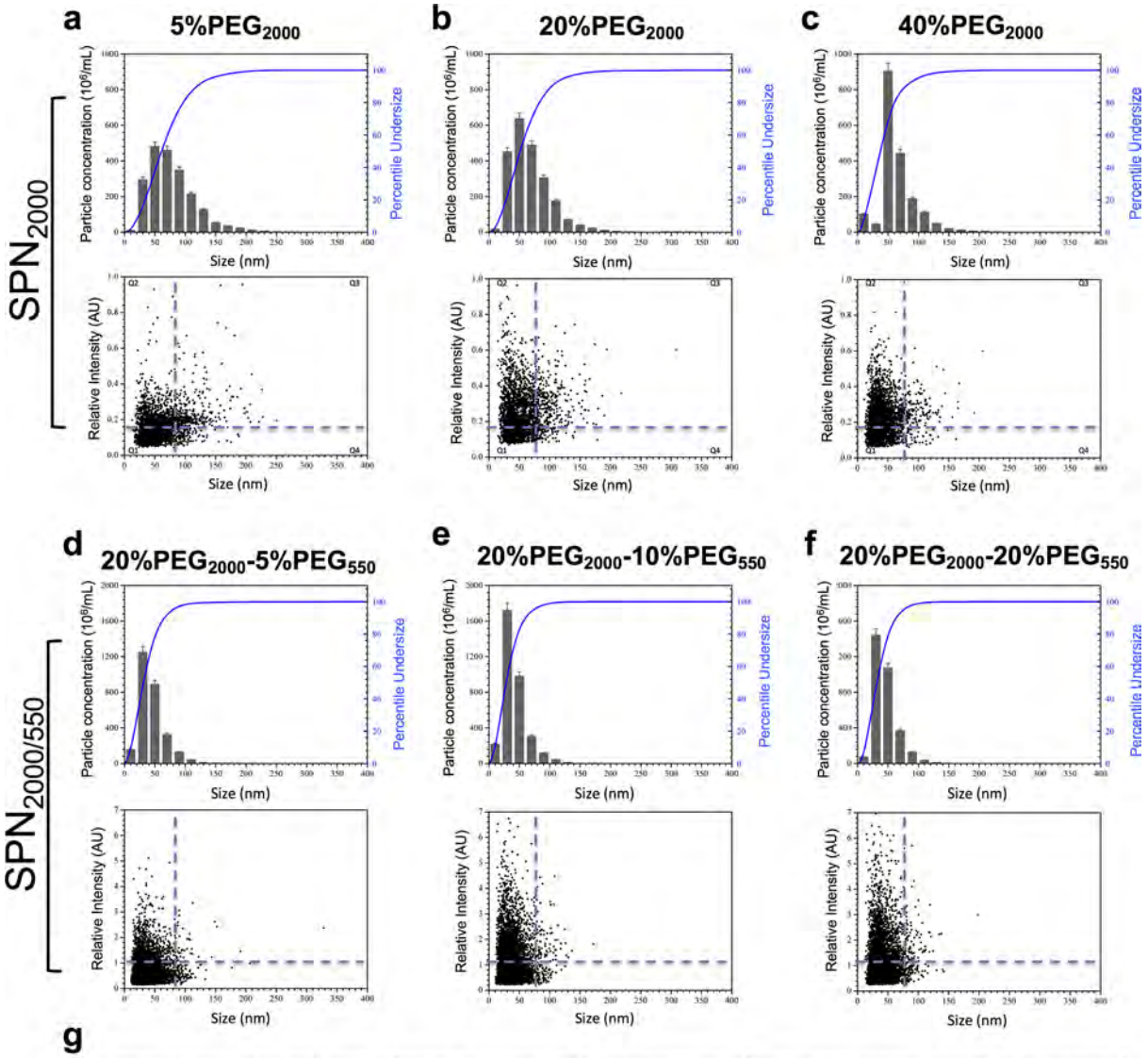

g

	Sample	NTA Mode (nm)	NTA Mean size (nm)	Number (x10^{12})/mL	DLS Mean size (nm) Polydispersity index	ζ (mV)
SPN_{2000}	$5\%PEG_{2000}$	53 ± 5	81 ± 5	0.697 ± 0.082	68 ± 18 0.185 ± 0.040	-50.8 ± 2.3
	$20\%PEG_{2000}$	42 ± 5	68 ± 3	0.897 ± 0.080	64 ± 9 0.155 ± 0.017	-55.0 ± 2.6
	$40\%PEG_{2000}$	33 ± 1	52 ± 3	1.251 ± 0.034	70 ± 10 0.126 ± 0.019	-57.0 ± 1.0
$SPN_{2000/550}$	$20\%PEG_{2000}$- $5\%PEG_{550}$	32 ± 4	46 ± 1	1.162 ± 0.085	56 ± 1 0.112 ± 0.016	-65.0 ± 5.0
	$20\%PEG_{2000}$- $10\%PEG_{550}$	30 ± 2	40 ± 1	1.324 ± 0.067	56 ± 2 0.133 ± 0.021	-64.0 ± 6.0
	$20\%PEG_{2000}$- $20\%PEG_{550}$	36 ± 1	44 ± 1	1.175 ± 0.055	60 ± 2 0.113 ± 0.019	-53.0 ± 3.0

Figure 2. Size distribution profiles of different SPN_{2000} and $SPN_{2000/550}$ determined by nanoparticle tracking analysis (NTA). (a–c) Size distribution profile (top row) and 2D plots of relative light scattering intensity of particles versus the estimate of the particle size for different $SPNs_{2000}$ (bottom row). (d–f) Size distribution profile (top row) and 2D plots of relative light scattering intensity of particles versus the estimate of the particle size of different $SNP_{2000/550}$ (bottom row). (g) List of key geometrical features for SPNs determined via NTA and DLS analyses.

Nanoparticle size distribution was further studied by NTA. The data in Figure 2 present the particle size distribution versus nanoparticle concentration (top rows) and intensity of scattered light obtained in terms of particle concentrations versus size and

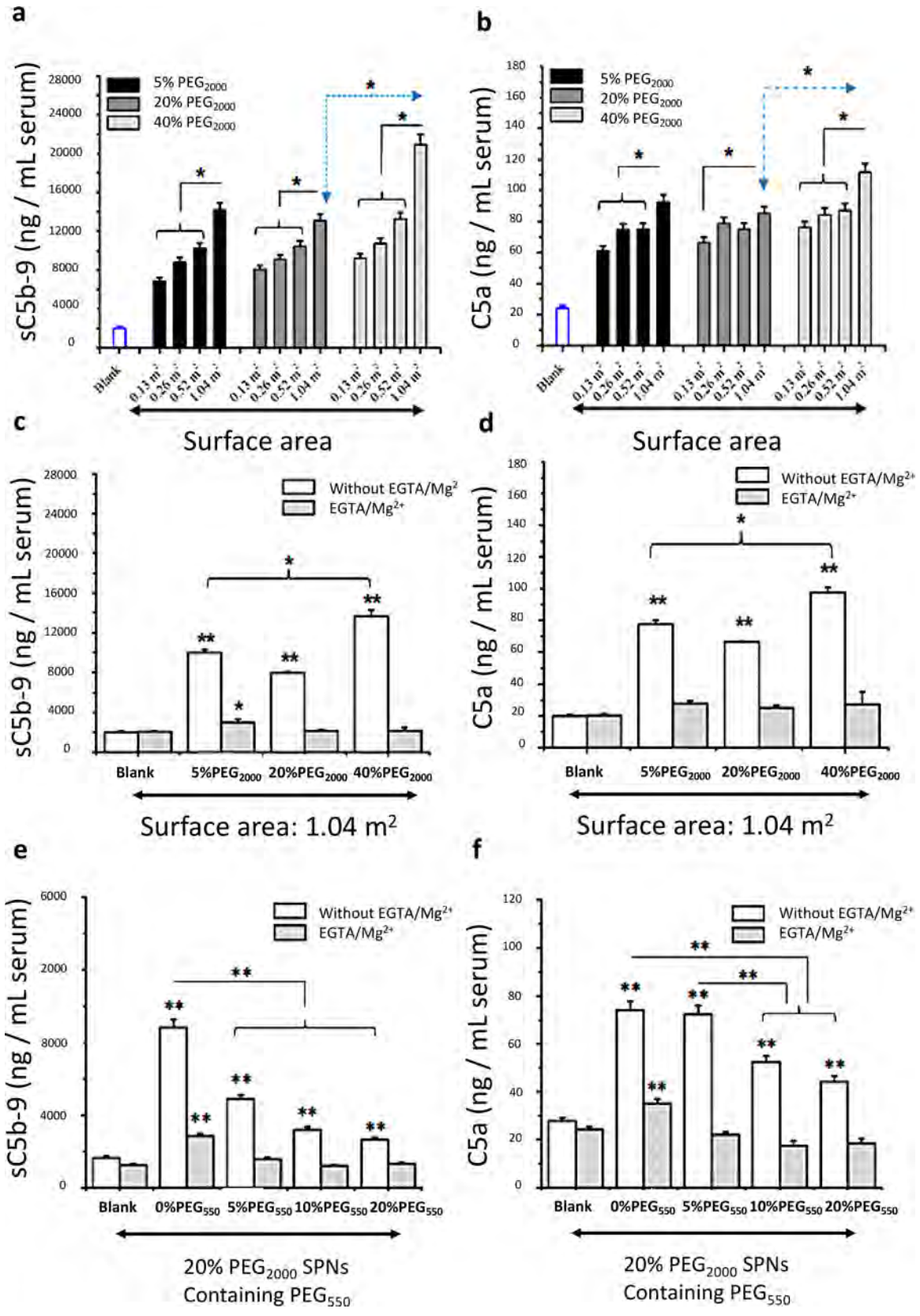

Figure 3. Mediated complement activation in human serum for SPNs. Panels (a) and (b) show surface-area-dependent SPN_{2000}-mediated increases of serum sC5b-9 and C5a above the background. Zymosan (1 mg/mL) was used as a positive control for monitoring complement activation. Panels (c) and (d) distinguish complement activation between calcium-sensitive pathways and the alternative pathway turnover. Panels (e) and (f) show serum sC5b-9 and C5a levels on $SPN_{2000/550}$ addition; $*p < 0.05$; $**p < 0.01$. Similar results were obtained in three other tested sera.

overall size distribution (bottom rows). For SPN_{2000}, NTA revealed a decrease in SPN mean size on increasing PEG_{2000} content (Figure 2a–c). Specifically, the NTA particle mean size decreased from 81.0 ± 5.0 nm for the 5% PEG_{2000} to 68.0 ± 3.0 nm for the 20%PEG_{2000} and 52.0 ± 3.0 nm for the 40%PEG_{2000} (table in Figure 2g). The decreasing size trend is in line with a decrease in particle mode and further reflected in gradual loss of nanoparticle subpopulations larger than 100 nm in size, an overall increase in particle number, and a more negative ζ-potential (table in Figure 2g). The proportion of nanoparticle subpopulation >100 nm were ∼20% for the 5% PEG_{2000}, became ∼10% for the 20%PEG_{2000}, and, eventually, ∼5% for 40% PEG_{2000} (Figure 2a–c, top row). Scatterplots of relative intensity versus particle size further show an increase in the proportion of nanoparticles <80 nm in size, with higher scattering above the median scattering intensity (>0.175 arbitrary unit; Q1 and Q2 quadrants) (Figure 2a–c, bottom row). Considering the significant increase in nanoparticle numbers on increasing carboxyPEG content, the observed changes in ζ-potential values may indicate changes in surface-projected PEG conformation with better exposure of carboxylic acid functionality (i.e., a more stretched "brush-like" configuration). In contrast to NTA, DLS measurements (table inset in Figure 2g) registered comparable mean sizes for all three SPN preparations but with considerably higher values than with NTA. These discrepancies may be due to the polydisperse nature of SPN suspensions and presence of a fraction of nanoparticles >80 nm in size, as the measure of total scattered light from an ensemble of SPNs in DLS is heavily weighted toward larger particles.[16] NTA size estimates are generally more accurate because, unlike DLS, NTA measures the Brownian motion by tracking the movement of individual particles.[16] Nevertheless, the decrease in polydispersity index on increasing carboxyPEG levels is in line with NTA observations.

On PEG pairing, the presence of 5% PEG_{550} dramatically reduced mean sizes from 68.0 ± 3.0 nm for SPN_{2000} with 20% PEG_{2000} and 0% PEG_{550} to 46 ± 1 nm for $SPN_{2000/550}$ with 5% PEG_{550}, as determined via NTA (table inset in Figure 2g). For the other two combinations, corresponding to 10 and 20% PEG_{550}, the mean NTA particle size was very similar to values of 40 ± 1 and 44 ± 1 nm, respectively. This was again reflected in nanoparticle mode reduction, an increase in nanoparticle number, and a more negative ζ-potential (table in Figure 2g). As such, in the $SPN_{2000/550}$, PEG_{2000} chains are expected to be laterally supported and constrained by the short and more "rigid" PEG_{550} chains. This would lead to a more compact and tightly packed configuration, where the PEG_{2000} chains would extend away from the particle surface in a stable but more stretched "brush-like" conformation with exposed carboxy termini. Differently, in the SPN_{2000}, the long and more flexible PEG_{2000} chains are expected to partially collapse on the nanoparticle surface, leading to a "mushroom-like" and/or "mushroom-brush" conformation with partially exposed carboxy moieties. This would explain the differences in hydrodynamic size and surface ζ-potential documented above in the side-by-side comparison between SPN_{2000} and $SPN_{2000/550}$. A further increase in PEG content, however, did not dramatically affect nanoparticle properties. The significant size reduction in PEG-paired $SPN_{2000/550}$ compared with SPN_{2000} may further imply higher nanoparticle stability.

The NTA results also show that nanoparticle mean size, mode, and total concentration remain comparable for all three different $SPN_{2000/550}$ configurations. However, increasing the PEG_{550} content increases the proportion of nanoparticles smaller than 80 nm in size with higher scattering above median scattering intensity (>1 arbitrary unit; Q1 and Q2 quadrants). Another exception is a substantial decrease in ζ-potential when PEG_{550} content is increased to 20%. The reason for this is unclear but may be a reflection of some PEG_{2000} conjugate displacement from the surface by increasing numbers of PEG_{550} molecules that compete better for the available space. The observed trends in NTA are also reflected in DLS studies confirming smaller mean sizes and narrower polydispersity on PEG pairing compared with the corresponding native SPN_{2000} carrying 20% PEG_{2000}. Finally, serum stability of SPNs was assessed in diluted (50% v/v) and undiluted fetal bovine serum at 37 °C. There was no observable sign of nanoparticle aggregation within 2 h of incubation in serum compared with non-PEGylated SPNs, which rapidly aggregated (Figure S3).

Nanoparticle-mediated complement activation in human sera was assessed by monitoring the generation of anaphylatoxin C5a and the soluble form of C5b-9 (sC5b-9), which are the two established markers of the terminal pathway of the complement system.[3] The results in Figure 3 show nanoparticle-mediated increases of C5a and sCb-9 on the basis of equivalent surface area (estimated through NTA). For each nanoparticle type, increasing surface area resulted in higher generation of both markers (Figure 3a,b). At the highest surface area tested (1.04 m^2/mL serum), complement activation was more profound with 40% PEG_{2000} SPNs compared with the corresponding nanoparticles of lower PEG content. This may be a reflection of the smaller size of 40% PEG_{2000} SPNs as compared to 20 and 5% PEG_{2000} SPNs, as nanoparticle curvature plays a significant role in modulating the conformation of bound immunoglobulins and/or complement sensing molecules. For instance, nanoparticle size was shown to affect IgM binding and conformation,[17] where adsorbed IgM on smaller nanoparticles (e.g., 100 nm) is strained and assumes a staple conformation that triggers activation of the first complement protein (C1) and hence activation of the classical pathway. On the other hand, adsorbed IgM on larger nanoparticles assumes a planar conformation, which does not activate C1.[17] The results in Figure 3c,d further show that complement activation by all SPNs is Ca^{2+}-dependent and does not involve any direct activation through the alternative pathway, which is Mg^{2+}-dependent.[3]

In contrast to mono-PEGylated nanoparticles, PEG pairing dramatically reduced complement activation (Figure 3e,f), where incorporation of a minimum of 10% PEG_{550} was sufficient to dramatically decrease C5a and sC5b-9 generation; however, with inclusion of 20% PEG_{550}, complement inhibition became more profound. The $SPN_{2000/550}$ with 20% PEG_{2000} and 20% PEG_{550} hold a total of 5.22×10^{16} PEG-phospholipid molecules/mg nanoparticle, which is slightly more than 20% PEG_{2000} SPN (4.33×10^{16} PEG-phospholipid molecules/mg nanoparticle) but considerably lower than 40% PEG_{2000} SPN (8.66×10^{16} PEG-phospholipid molecules/mg nanoparticle), yet this intermediate PEG lipid level substantially overcomes complement activation. By considering the observation that these nanoparticles exhibit similar size distribution profiles, the observed reduction in complement activation is presumably the result of altered PEG_{2000} spacing and stretching on PEG pairing. Thus, PEG stretching might not only have generated end-terminal carboxy clusters of appropriate architecture that overcomes complement activation[14] but also could have limited protein intercalation into PEG_{2000} cloud, thereby sterically minimizing complement convertase assembly.

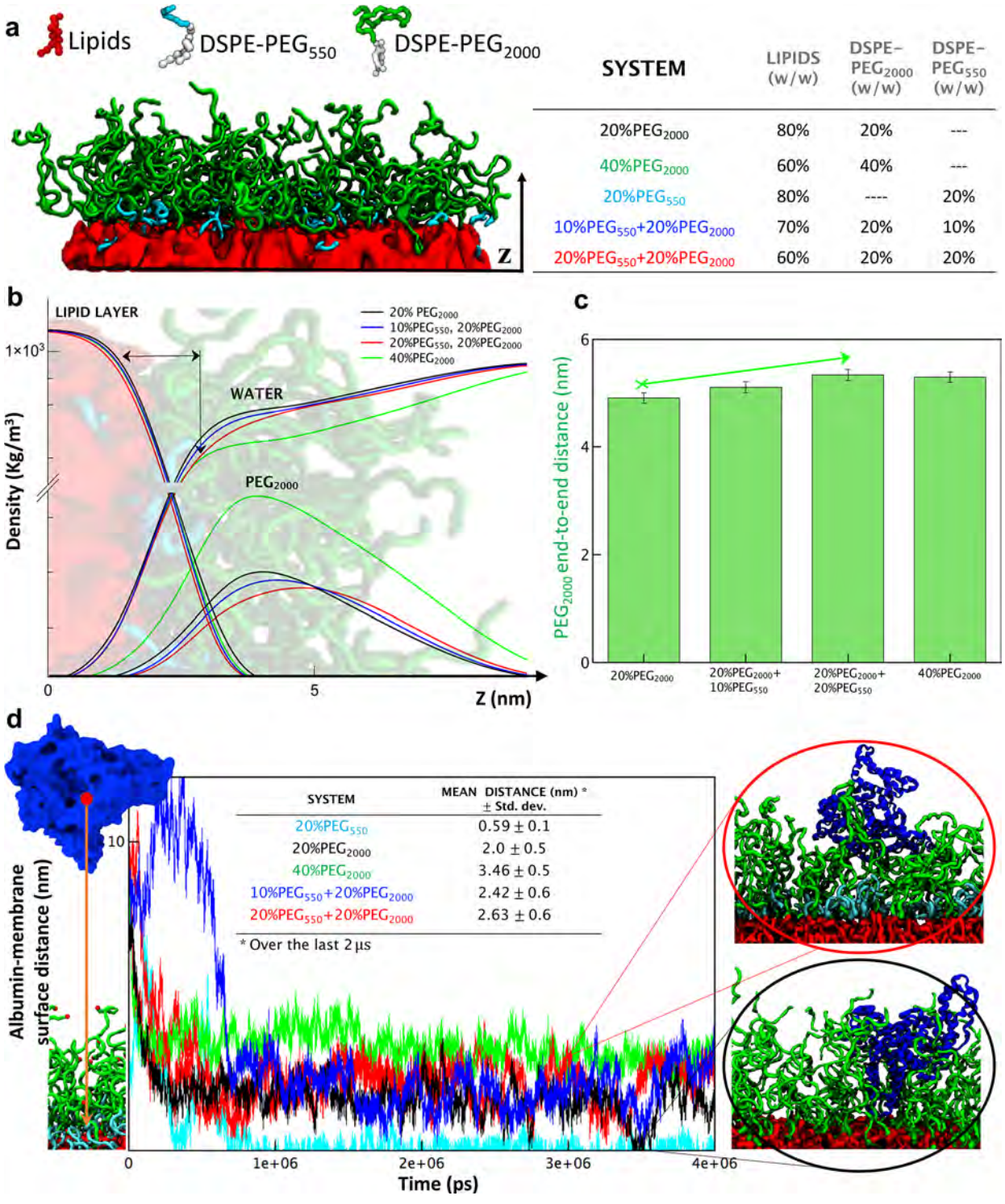

Figure 4. Molecular dynamics simulations for PEG-paired SPNs. (a) Computational domain (left) for the 20% PEG_{550} configuration, including PEG_{2000} chains (green), PEG_{550} chains (cyan), and lipids (red). List of different computed configurations (right). (b) Density of lipids (lipid layer line), water molecules (water line), and PEG_{2000} (PEG_{2000} line) is plotted along the *z*-coordinate, normal to the surface (20% PEG_{2000}, black; 10% PEG_{550}-20% PEG_{2000}, blue; 20% PEG_{550}-20% PEG_{2000}, red40% PEG_{2000}, green). (c) End-to-end distance for PEG_{2000} chains. (d) Distance between an albumin molecule (blue) and the center of mass of the lipid layer headgroups over a period of 4 μs. The table inset shows mean distance values computed over the last 2 μs. The black circle inset shows an albumin molecule interacting with a 20% PEG_{2000} platform. The red circle inset depicts an albumin molecule interacting with a 20% PEG_{2000}-20% PEG_{550}. These images were back-mapped from a coarse-grained to an atomistic representation (gromos54a7 force field).[28]

PEG pairing had no direct effect on alternative pathway activation, as complement activation was halted in the presence of EGTA/Mg^{2+} (Figure 3e,f). To delineate the role of calcium-sensitive pathways, complement experiments were repeated with both 20% PEG_{2000} nanoparticles and $SPN_{2000/550}$ (20% carboxyPEG_{2000} and 20% methoxyPEG_{550}) in the presence of

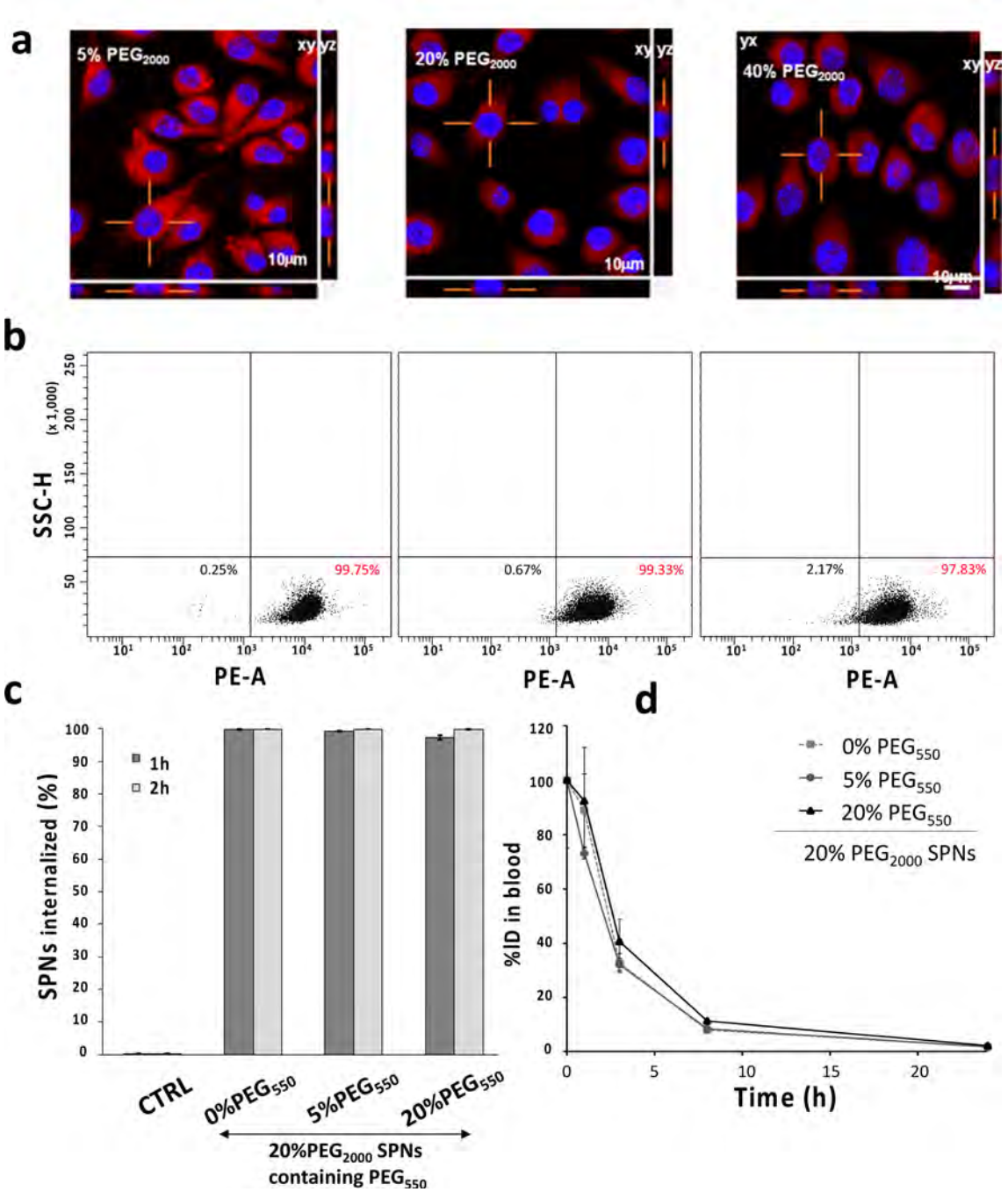

Figure 5. Cell uptake and in vivo blood longevity of SPNs. (a) Confocal microscopy images of J-774.A1 macrophages incubated for 2 h with 5, 20, and 40% PEG_{2000} SPNs (SPN_{2000} is labeled with red fluorescent dye (PE-RhB), and cell nuclei are labeled with 4′,6-diamidino-2-phenylindole). (b) Flow cytometry analysis showing the extent of $SPN_{2000/550}$ association with J-774.A1 cells at 1 h postincubation. (c) Flow cytometry analysis of $SPN_{2000/550}$ association with J-774.A1 phagocytes at 1 and 2 h postincubation, as a function of the PEG_{550} content (0, 5, and 20%). In all cases, nanoparticles carried 20% PEG_{2000}. (d) Blood concentration of Cu^{64}-labeled SPN_{2000} and $SPN_{2000/550}$, with different PEG_{550} content (0, 5, and 20%) in healthy mice following tail-vein injection (n = 3).

2.25 μM (final concentration) C1 esterase inhibitor (an inhibitor of the classical pathway components C1r and C1s, the contact system, and fibrinolytic proteases).[10] With all nanoparticle types, no inhibition was observed and equivalent quantities of C4d (an established marker for activation of both classical and lectin pathways)[3] were liberated (serum C4d background level of 3.8 ± 1.1, and 12.8 ± 1.6 and 13.2 ± 0.9 μg/mL C4d in the absence and presence of C1 esterase inhibitor for 20% PEG_{2000} nanoparticles, and 4.9 ± 0.6 and 4.7 ± 0.9 μg/mL C4d in the absence and presence of C1 esterase inhibitor for $SPN_{2000/550}$, respectively). These observations not only exclude the role of classical pathway in complement activation but also confirm the lesser ability of PEG-paired nanoparticles in activating complement. Therefore, the observed complement activation is most likely through the lectin pathway, and this is further supported by lack of C4d liberation on nanoparticle addition to serum pretreated with Futhan (150 μg/mL), which is a broad-spectrum serine protease inhibitor capable of

inhibiting lectin pathway mannose-binding lectin (MBL) (or collectins/ficolins)/MBL-associated serine proteases (MBL-MASPs) (2.8 ± 0.6, 3.1 ± 0.5, and 3.3 ± 0.8 μg/mL for background, 20% PEG_{2000} and 20% PEG_{2000}/20% PEG_{550}-paired nanoparticles, respectively). Therefore, PEG pairing interferes with the action of MBL/ficolins/collectins-MASPs, presumably by minimizing their intercalation into the PEG cloud.

To further gain insight into the above-mentioned observations, coarse-grained molecular dynamics (MD) simulations within the Martini framework[18,19] were performed to predict the organization of PEG chains and the interaction with blood molecules. Following the experimental cases above, five different configurations were tested (Figure 4a): 20% PEG_{2000} and 40% PEG_{2000}, representing conventional camouflaging approaches with long PEG chains solely; 10% PEG_{550}-20% PEG_{2000} and 20% PEG_{550}-20% PEG_{2000}, representing PEG pairing approaches with short and long PEG chains together; 20% PEG_{550}, representing a control configuration with low-density, short PEG chains.

The results of the simulations are presented in Figure 4b in terms of lipid concentration, water molecules, and PEG_{2000} content along the z-coordinate. Moving away from the surface, a sharp decrease in lipid concentration from 1100 kg/m^3 on the innermost layer to 0 at about 3.5 nm, an increase in the density of water molecules from nearly 0 in the core to ~1000 kg/m^3 in the bulk fluid, and a biphasic variation in PEG_{2000} density reaching a maximum of 4−5 nm are observed. The sharp reduction in the lipid content is ascribed to the fact that lipid chains are localized only in the innermost layer (red layer in Figure 4a), whereas the outer region is mostly occupied by polymer chains and water molecules. Significant variations for the water and PEG concentrations are observed for all configurations. Specifically, as the concentration of PEG_{2000} and PEG_{550} increases, the density of water molecules adjacent to the lipid layer ($z > 2$) decreases, whereas the center of mass for the PEG_{2000} distribution progressively moves toward larger z values (from 4 to 5 nm). Importantly, for the 20% PEG_{550}-20% PEG_{2000} paired configuration, the maximum PEG_{2000} density is at $z = 5$ nm. Simulations also allowed the end-to-end distance for the PEG_{2000} chains (Figure 4c) to be quantified. For the 20% PEG_{550}-20% PEG_{2000} configurations, PEG_{2000} chains appeared more elongated with an end-to-end distance of 5.3 ± 0.1 nm as compared to the conventional system, 20% PEG_{2000}, returning a value of 4.9 ± 0.1 nm. Collectively, these results further support the notion that the inclusion of PEG_{550} guides the PEG_{2000} chains to predominantly display a "stretched brush-like" architecture.

MBL/ficolins/collectins-MASPs are large complexes, and their intercalation into the PEG cloud is expected to be more challenging compared with smaller proteins, such as albumin. Thus, in order to estimate the effect of PEG conformational displays on protein intercalation, the separation distance between albumin molecules and the lipid layer was monitored over time for the five different cases (Figure 4d). MD simulations predicted three distinct behaviors: protein adsorption at the PEG coating−water interface, partial protein intercalation within the PEG chains, and deep protein intercalation into the PEG cloud. At the first instance, protein persistence at particle surfaces is modulated by chain mobility and softness of the PEG outer layer.[20,21] At the PEG−water interface (between 5 and 10 nm), the paired combination of 20% PEG_{550}-20% PEG_{2000} induced an overall larger fluctuation in albumin separation distance compared with conventional 20% PEG_{2000} and 40% PEG_{2000} platforms (Figure S4). This would suggest an overall higher outer-layer deformability for the PEG-paired configuration that could more efficiently repel any approaching protein and possibly limit protein intercalation. At the opposite extreme, albumin would intercalate deep into the PEG cloud in the case of a low-density, short PEG_{550} configuration (20%PEG_{550} cyan line in Figure 4d). A similar behavior was also observed with the 20%PEG_{2000} configuration, displaying a low-density, long PEG_{2000} chains (black line in Figure 4d). As short PEG_{550} chains were inserted into a lipid layer with 20% PEG_{2000}, albumin intercalation was delayed and occurred partially (10% PEG_{550}-20% PEG_{2000}, blue line, and 20% PEG_{550}-20% PEG_{2000}, red line, in Figure 4d and Movie S1 and Movie S2, respectively). A maximum in steric hindrance was observed in the case of lipid platforms exhibiting 40% PEG_{2000} (green line in Figure 4d) for which the separation distance of the albumin from the lipid layer was only slightly larger than that in the case of the PEG-paired 20% PEG_{550}-20% PEG_{2000} (red line in Figure 4d). It should be emphasized that, although the dense 40% PEG_{2000} surfaces appear to block more efficiently albumin intercalation compared with the PEG-paired 20% PEG_{550}-20% PEG_{2000} platforms, simulations do not account for the contribution of surface curvature on PEG conformation or the overall particle stability in suspension. On a curved surface, the projected long PEG_{2000} chains would tend to open up more than short PEG_{550} chains, thus facilitating protein intercalation. Collectively, these simulations would indicate that surface PEG pairing efficiently limits binding and/or intercalation of medium- and small-sized proteins compared to PEG_{2000}-grafted surfaces. Indeed, this is in line with the complement activation studies documented in Figure 3 and would support the notion that MBL/ficolins/collectins-MASPs intercalation into the PEG-paired cloud is impaired.

It has long been known that the steric hindrance of the surface-projected PEG chains can minimize nanoparticle−phagocyte contact, despite opsonization.[22] Accordingly, we sought to investigate whether PEG pairing can suppress nanoparticle uptake by J-774.A1 macrophages (which express complement receptor 3). The data in Figure 5a support the suppressive effect of increasing PEG_{2000} density on SPN_{2000} internalization by macrophages (reduced red fluorescent intensity with increasing PEG_{2000} surface density from 5 to 40%). Thus, by considering that complement activation (and presumably C3b/iC3b opsonization) proceeds better with 40% PEG_{2000} SPNs compared with nanoparticles of lower PEG density (Figure 3), these observations confirm that PEG conformation (and steric hindrance) plays a modulatory role in nanoparticle−cell interaction and therefore interfere with ligation of surface-bound opsonins with macrophage receptors. Flow cytometry was also employed to quantitatively determine differences in cell uptake between 20% PEG_{2000} SPNs and PEG-paired nanoparticles. No significance difference was detected among 20% PEG_{2000} SPNs and 20% PEG_{2000} SPNs carrying either 5 or 20% PEG_{550} (Figure 5b,c). Again, this supports the notion that the PEG steric barrier is the dominant factor in modulating the extent of nanoparticle−cell interaction,[22] and its efficacy remains unaffected on surface PEG pairing. In line with these observations, comparable blood clearance kinetics was also observed between single and PEG-paired Cu^{64}-DOTA-labeled SPNs upon intravenous injection (Figure 5d). The blood clearance kinetics is similar to the previously described PEGylated nanosystems.[23,24] In this respect, it is important to

highlight that the proposed PEG-pairing is different from other hierarchical PEG surface structures, such as the double-PEG layer,[21] in that the main objective here is minimizing complement activation.

In conclusion, this report showed that surface PEG pairing of nanoparticles could minimize complement activation without further affecting macrophage clearance and circulation profile. Considering these properties and the observation that PEG-pair-stabilized SPNs generate considerably less C5a in comparison to conventional PEGylated species, PEG pairing may offer a better strategy for design and engineering of safer nanomedicines. Indeed, intratumoral complement activation by extravasated PEGylated nanomedicines could potentially promote tumor growth, as the buildup of a sufficient C5a gradient helps with recruitment of immunosuppressive cells.[25,26] Thus, PEG pairing may be considered as an alternative cost-effective approach for overcoming complement activation compared with nanoparticles grafted with complement inhibitors. Finally, the residual level of complement activation products by PEG-paired SPNs may be ascribed to the heterogeneity of the current system and presumably arising from the presence of a small subpopulation of larger nanoparticles (>80 nm) with poorer PEG shielding. Improved nanoprecipitation procedures (e.g., through microfluidic processes)[27] may eventually yield a more homogeneous population of complement-evading PEG-paired nanoparticles.

Supporting Information

The Supporting Information is available free of charge at https://pubs.acs.org/doi/10.1021/acs.nanolett.0c01011.

Movie S1: Coarse-grained simulations for the interaction of an albumin molecule on PEG2000-stabilized surfaces; albumin intercalates into the PEG chains reaching the lipid surface (AVI)

Movie S2: Coarse-grained simulations for the interaction of an albumin molecule on PEG2000/550-stabilized surfaces; albumin tends to accommodate at the center of the PEG monolayer without reaching the lipid surface (AVI)

Materials and methods and supporting Figures S1−S4 (PDF)

Corresponding Authors

Seyed Moein Moghimi − *School of Pharmacy and Translational and Clinical Research Institute, Newcastle University, Newcastle upon Tyne NE1 7RU, United Kingdom*;
Email: seyed.moghimi@ncl.ac.uk

Paolo Decuzzi − *Laboratory of Nanotechnology for Precision Medicine, Fondazione Istituto Italiano di Tecnologia, 16163 Genoa, Italy*; orcid.org/0000-0001-6050-4188;
Email: paolo.decuzzi@iit.it

Author Contributions

M.P., S.E., and L.-P.W. share first authorship. S.M.M. and P.D share senior authorship. M.P. performed MD simulations; S.E., J.K., and S.A. synthesized and characterized SPNs; L.-P.W. performed complement and NTA studies; all authors contributed to experimental planning and data analysis. S.M.M. and P.D. conceived the idea, supervised the work, and wrote the manuscript with contributions from all coauthors.

■ ACKNOWLEDGMENTS

This project was partially supported by the European Research Council, under the European Union's Seventh Framework Programme (FP7/2007-2013)/ERC Grant Agreement No. 616695, by the Italian Association for Cancer Research (AIRC) under the individual investigator Grant No. 17664, and by the European Union's Horizon 2020 research and innovation programme under the Marie Sklodowska-Curie Grant Agreement No. 754490 - MINDED. S.M.M. and L-P.W. further acknowledge financial support by International Science and Technology Cooperation Project of HuangPu (No. 2018GH15), Guangzhou City, with RiboBio Co. Ltd., China.

■ REFERENCES

(1) Ricklin, D.; Hajishengallis, G.; Yang, K.; Lambris, J. D. Complement: a key system for immune surveillance and homeostasis. *Nat. Immunol.* **2010**, *11*, 785−797.

(2) Holers, V. M. Complement and its Receptors: New Insights into Human Disease. *Annu. Rev. Immunol.* **2014**, *32*, 433−459.

(3) Hamad, I.; Al-Hanbali, O.; Hunter, A. C.; Rutt, K. J.; Andresen, T. L.; Moghimi, S. M. Distinct Polymer Architecture Mediates Switching of Complement Activation Pathways at the Nanosphere-Serum Interface: Implications for Stealth Nanoparticle Engineering. *ACS Nano* **2010**, *4*, 6629−6638.

(4) Coty, J. B.; Eleaman Oliveira, E.; Vauthier, C. uning Complement Activation and Pathway through Controlled Molecular Architecture of Dextran Chains in Nanoparticle Corona. *Int. J. Pharm.* **2017**, *532*, 769−778.

(5) Yu, K.; Lai, B. F. L.; Foley, J. H.; Krisinger, M. J.; Conway, E. M.; Kizhakkedathu, J. N. Modulation of Complement Activation and Amplification on Nanoparticle Surfaces by Glycopolymer Conformation and Chemistry. *ACS Nano* **2014**, *8*, 7687−7703.

(6) Chen, F. F.; Wang, G. K.; Griffin, J. I.; Brenneman, B.; Banda, N. K.; Holers, V. M.; Backos, D. S.; Wu, L. P.; Moghimi, S. M.; Simberg, D. Complement proteins bind to nanoparticle protein corona and undergo dynamic exchange in vivo. *Nat. Nanotechnol.* **2017**, *12*, 387−393.

(7) Vu, V. P.; Gifford, G. B.; Chen, F.; Benasutti, H.; Wang, G.; Groman, E. V.; Scheinman, R.; Saba, L.; Moghimi, S. M.; Simberg, D. Immunoglobulin deposition on biomolecule corona determines complement opsonization efficiency of preclinical and clinical nanoparticles. *Nat. Nanotechnol.* **2019**, *14*, 260−268.
(8) Needham, D.; McIntosh, T. J.; Lasic, D. D. Repulsive Interactions and Mechanical Stability of Polymer-Grafted Lipid Membranes. *Biochim. Biophys. Acta, Biomembr.* **1992**, *1108*, 40−48.
(9) Moghimi, S. M.; Simberg, D. Complement activation turnover on surfaces of nanoparticles. *Nano Today* **2017**, *15*, 8−10.
(10) Moghimi, S. M. The effect of methoxy-PEG chain length and molecular architecture on lymph node targeting of immuno-PEG liposomes. *Biomaterials* **2006**, *27*, 136−44.
(11) Aryal, S.; Key, J.; Stigliano, C.; Ananta, J. S.; Zhong, M.; Decuzzi, P. Engineered magnetic hybrid nanoparticles with enhanced relaxivity for tumor imaging. *Biomaterials* **2013**, *34*, 7725−32.
(12) Aryal, S.; Key, J.; Stigliano, C.; Landis, M. D.; Lee, D. Y.; Decuzzi, P. Positron emitting magnetic nanoconstructs for PET/MR imaging. *Small* **2014**, *10*, 2688−96.
(13) Stigliano, C.; Key, J.; Ramirez, M.; Aryal, S.; Decuzzi, P. Radiolabeled Polymeric Nanoconstructs Loaded with Docetaxel and Curcumin for Cancer Combinatorial Therapy and Nuclear Imaging. *Adv. Funct. Mater.* **2015**, *25*, 3371−3379.
(14) Wibroe, P. P.; Mat Azmi, I. D.; Nilsson, C.; Yaghmur, A.; Moghimi, S. M. Citrem modulates internal nanostructure of glyceryl monooleate dispersions and bypasses complement activation: Towards development of safe tunable intravenous lipid nanocarriers. *Nanomedicine* **2015**, *11*, 1909−1914.
(15) Sou, K.; Tsuchida, E. Electrostatic interactions and complement activation on the surface of phospholipid vesicle containing acidic lipids: effect of the structure of acidic groups. *Biochim. Biophys. Acta, Biomembr.* **2008**, *1778*, 1035−1041.
(16) Wright, M. Nanoparticle Tracking Analysis for the Multiparameter Characterization and Counting of Nanoparticle Suspensions. *Nanoparticles in Biology and Medicine*; Springer, 2012; pp 511−524.
(17) Pedersen, M. B.; Zhou, X.; Larsen, E. K.; Sorensen, U. S.; Kjems, J.; Nygaard, J. V.; Nyengaard, J. R.; Boesen, T.; Vorup-Jensen, T. Curvature of synthetic and natural surfaces is an important target feature in classical pathway complement activation. *J. Immunol.* **2010**, *184*, 1931−1945.
(18) Marrink, S. J.; Risselada, H. J.; Yefimov, S.; Tieleman, D. P.; de Vries, A. H. The MARTINI force field: coarse grained model for biomolecular simulations. *J. Phys. Chem. B* **2007**, *111*, 7812−24.
(19) Grunewald, F.; Rossi, G.; de Vries, A. H.; Marrink, S. J.; Monticelli, L. Transferable MARTINI Model of Poly (ethylene Oxide). *J. Phys. Chem. B* **2018**, *122*, 7436−7449.
(20) Liu, D.; Guo, J.; Zhang, J.-H. Chain mobility and film softness mediated protein antifouling at the solid−liquid interface. *J. Mater. Chem. B* **2016**, *4*, 6134−6142.
(21) Zhou, H.; Fan, Z.; Li, P. Y.; Deng, J.; Arhontoulis, D. C.; Li, C. Y.; Bowne, W. B.; Cheng, H. Dense and dynamic polyethylene glycol shells cloak nanoparticles from uptake by liver endothelial cells for long blood circulation. *ACS Nano* **2018**, *12*, 10130−10141.
(22) Dos Santos, N.; Allen, C.; Doppen, A.-M.; Anantha, M.; Cox, K. A.K.; Gallagher, R. C.; Karlsson, G.; Edwards, K.; Kenner, G.; Samuels, L.; Webb, M. S.; Bally, M. B. Influence of Poly(Ethylene Glycol) Grafting Density and Polymer Length on Liposomes: relating Plasma Circulation Lifetimes to Protein Binding. *Biochim. Biophys. Acta, Biomembr.* **2007**, *1768*, 1367−1377.
(23) Pasut, G.; Paolino, D.; Celia, C.; Mero, A.; Joseph, A. S.; Wolfram, J.; Cosco, D.; Schiavon, O.; Shen, H.; Fresta, M. Polyethylene glycol (PEG)-dendron phospholipids as innovative constructs for the preparation of super stealth liposomes for anticancer therapy. *J. Controlled Release* **2015**, *199*, 106−113.
(24) Paolino, D.; Cosco, D.; Racanicchi, L.; Trapasso, E.; Celia, C.; Iannone, M.; Puxeddu, E.; Costante, G.; Filetti, S.; Russo, D.; Fresta, M. Gemcitabine-loaded PEGylated unilamellar liposomes vs GEMZAR (R): Biodistribution, pharmacokinetic features and in vivo antitumor activity. *J. Controlled Release* **2010**, *144*, 144−150.
(25) Moghimi, S. M. Cancer nanomedicine and the complement system activation paradigm: anaphylaxis and tumour growth. *J. Controlled Release* **2014**, *190*, 556−62.
(26) Ajona, D.; Ortiz-Espinosa, S.; Pio, R. Complement Anaphylatoxins C3a and C5a: Emerging Roles in Cancer Progression and Treatment. *Semin. Cell Dev. Biol.* **2019**, *85*, 153−163.
(27) Valencia, P. M.; Farokhzad, O. C.; Karnik, R.; Langer, R. Microfluidic technologies for accelerating the clinical translation of nanoparticles. *Nat. Nanotechnol.* **2012**, *7*, 623−9.
(28) Oostenbrink, C.; Villa, A.; Mark, A. E.; van Gunsteren, W. F. A biomolecular force field based on the free enthalpy of hydration and solvation: the GROMOS force-field parameter sets 53A5 and 53A6. *J. Comput. Chem.* **2004**, *25*, 1656−76.